Design of a Brushless PM Starter-Generator for Low-Cost Manufacture and a High-Aspect-Ratio Mechanical Space Envelope

Rafal Wrobel, Nick Simpson, Phil H. Mellor
Department of Electrical & Electronic Engineering
University of Bristol, Bristol, UK
r.wrobel@bristol.ac.uk
n.simpson@brsitol.ac.uk
p.h.mellor@brsitol.ac.uk

James Goss, Dave A. Staton
Motor Design Ltd., Ellesmere, UK
james.goss@motor-design.com
dave.staton@motor-design.com

***Abstract*— This paper presents the results of a brushless PM starter-generator design which caters for low-cost manufacture and a highly constrained mechanical space-envelope. The starter-generator design addresses the low-cost requirement through the use of aluminium winding conductors and ferrite permanent magnets. This presents several challenges which include, but are not limited to, the selection of an appropriate machine topology to realise a high specific output with the lower performance materials, minimising the power losses associated with the higher resistivity of aluminium and the enhancement of thermal performance. The problem is further exacerbated by the demanding space-envelope, operating requirements and the necessity of 'design for manufacture'. The selection of an appropriate machine topology is paramount in the present application as the limited mechanical space-envelope results in a 'pancake' like geometry in which the aspect ratio of the stator outer diameter to the machine active length is high. To provide a solution satisfying all these challenging design requirements an approach combining the theoretical electromagnetic and thermal analyses together with tests on machine subassemblies has been employed here. Such a method allows for a more informed design process, where the manufacture and assembly nuances affecting the starter-generator's performance are identified and accounted for prior to prototyping of the complete machine assembly. The paper discusses the employed design methodology in detail. A number of machine designs with alternative winding constructions has been considered providing an insight into challenges and limitations for the cost-effective winding construction utilising aluminium conductors. The results from analysis of the starter-generator suggest that the proposed machine design is capable of achieving the design requirements for both continuous and transient operating modes.**

Keywords—PM starter-generator, design for manufacture, design for cost, low-cost aluminium winding, ferrite PM rotor;

I. INTRODUCTION

The design of electrical machines is a multi-disciplinary problem in which the various performance requirements such as torque-speed envelope, duty-cycle and thermal characteristics must be considered alongside specific design paradigms such as 'design for cost' or 'design for manufacture'. The various design factors limit the applicable solutions and so must be considered from the outset of the design process. The 'design for cost' and 'design for manufacture' paradigms have gained increasing interest, which is reflected in the available literature [1]-[12]. In particular, research into machine designs with reduced quantities of rare-earth PM materials achieved through the adoption of interior PM machine topologies or the use of alternative PM materials such as ferrites, Dysprosium-free or Dysprosium-less NdFeB. Furthermore, PM-free designs such as reluctance and synchronous reluctance machine topologies have received considerable attention [1]-[5]. The development of low-cost stator and winding topologies have been reported which allow for ease of manufacture and assembly while providing the required performance measures such as good heat extraction from the winding assembly and reduced winding power loss [6]-[12].

This paper presents an analysis of a brushless PM starter-generator design study which addresses 'design for cost' and 'design for manufacture' through the use of less expensive and more economically stable active materials and the adoption of simple manufacturing and assembly methods. A radial-flux machine topology with an open-slot stator structure accommodating pre-formed aluminium windings and an inner rotor with surface mounted ferrite PMs has been selected as a solution which meets the required low-cost manufacture and performance measures and is analysed in detail. The application of lower cost materials, which typically exhibit poorer material properties, leads to various design challenges and limitations with respect to the achievable machine performance for a given topology and mechanical space-envelope. To meet the challenging design requirements a design methodology utilising theoretical and experimental techniques has been adopted. The theoretical approach makes use of the finite element electromagnetic and thermal lumped-parameters equivalent-circuit methods. The experimental approach comprises tests on machine hardware subassemblies (motoretts). The stator winding subassembly has been found to be particularly useful in assessing various manufacture and assembly nuances affecting the power loss and heat transfer from the winding body into the machine periphery, which are notoriously difficult to derive

accurately using theoretical techniques [14], [23], [24], [26]. A detailed description of the design process supplemented with experimental and theoretical data has been provided in consecutive sections of the paper. A number of machine candidates utilising alternative winding constructions have been analysed. The results from theoretical analyses and tests on the motorettes' hardware highlight the major challenges and limitations for the cost-effective machine designs with aluminium windings. In addition, the results from the analysis of the starter-generator suggest that the proposed machine design is capable of achieving the design requirements for both continuous and transient operating modes.

II. Design Philosophy

The initial choice of machine topology has been dictated by the requirement of simple winding manufacture and assembly. Hence, a modular radial-flux machine topology with an open-slot stator and a preformed winding construction has been selected here. The preformed and/or compressed concentrated winding topology allows for the coils to be manufactured in isolation, in a simple and repeatable manner providing improved winding performance measures and manufacturability, as compared with other winding topologies [6], [8], [9], [12], [15], [25]. The preformed coils are then placed in the stator slots with an appropriate slot liner and secured with a slot wedge. The complete stator-winding assembly is then impregnated in order to improve the electrical insulation and the mechanical and thermal performance.

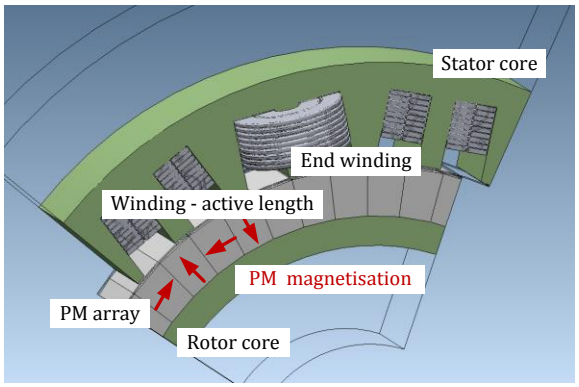

Fig. 1. Section of the starter generator geometry

Table I. Basic Motor Data

Package volumetric envelope	3.6 litres
Maximum rated rotational speed	5000 rpm
Nominal power/torque (continuous)	7.5 kW/30Nm
Peak transient power/torque	15 kW/60Nm
Nominal voltage	48 V

A variant of the 10 pole (p =10) 12 slot (q = 12) machine topology with a single-layer, three-phase concentrated winding is considered here, Fig. 1. Table I lists the basic motor data including the output power requirements and the mechanical space-envelope. The diameter to length aspect ratio is 9.4. The target magnetic and electrical loadings which satisfy the design requirements are B_1=0.4T and Q_{rms}=70,000A_{rms}/m respectively. These loading values are challenging when considering the properties of readily available low cost ferrite permanent magnets and the higher resistance of aluminium conductors. The limited active area combined with the relatively low magnetic loading leads to a target electric loading comparable to more conventional copper wound machine designs and consequently a large number of Ampere-turns per phase. The winding and core losses are additionally affected by the relatively high operating fundamental frequency, equal to approximately 1kHz for the high-end of the required torque-speed envelope. Furthermore, the phase inductance has to be limited ensuring the required peak power at higher operating speeds is within the inverter supply constraints. Therefore, in order to realise a feasible machine design each of the performance issues must to be addressed simultaneously.

The winding loss is managed across the entire torque-speed envelope by the choice of topology which allows for a large slot winding area and preformed coils. The arrangement of conductors within the stator slots has been defined to minimise ac effects and coil compression is employed to maximise the effective conductor fill factor, k_p. The iron loss is addressed by the use of 0.2 mm SiFe laminations in the stator and rotor core packs to reduce eddy-current loss at high-speed operation. The PM loss was found to be negligible due to the high electrical resistivity of the ferrite material, consequently the machine design effort has been focused on the stator-winding assembly, as the main source of loss.

In order to fully utilise the lower grade PM material and provide the required magnetic loading, a two-segment per pole discrete-Halbach PM array is adopted. Careful considerations must be made when designing a ferrite PM rotor array to avoid demagnetisation which can result from high electric loading combined with low temperature operation which is likely to occur in the present application. The complete PM array is composed from geometrically identical, trapezoidal shaped PM segments, which are retained with a non-magnetic sleeve. The sleeve provides a degree of mechanical retention in addition to adhesive bonding the PM array to the rotor back iron. The individual PM segments are magnetised normally or tangentially in reference to the rotor outer surface, as shown in Fig. 1. The trapezoidal shaped PM blocks enable simpler fabrication and better material utilisation as compared with more commonly used arc shaped PM segments.

Fig. 1 presents a schematic of the active elements, and illustrates the relatively short active length of the machine and the large end-windings of the preformed concentrated winding. A parallel-sided slot design is introduced to simplify the manufacture and assembly of the winding and to improve the heat transfer from the winding body into the stator and housing assembly [23]. Good thermal contact is particularly important as the machine housing is interfaced with a water jacket which provides the main dissipative path for the generated power loss.

III. Machine Prototyping

One of the vital components in the development of the starter-generator is the winding assembly. A number of coil constructions have been evaluated with respect to the generated loss and ease of manufacture. These include an edge-wound

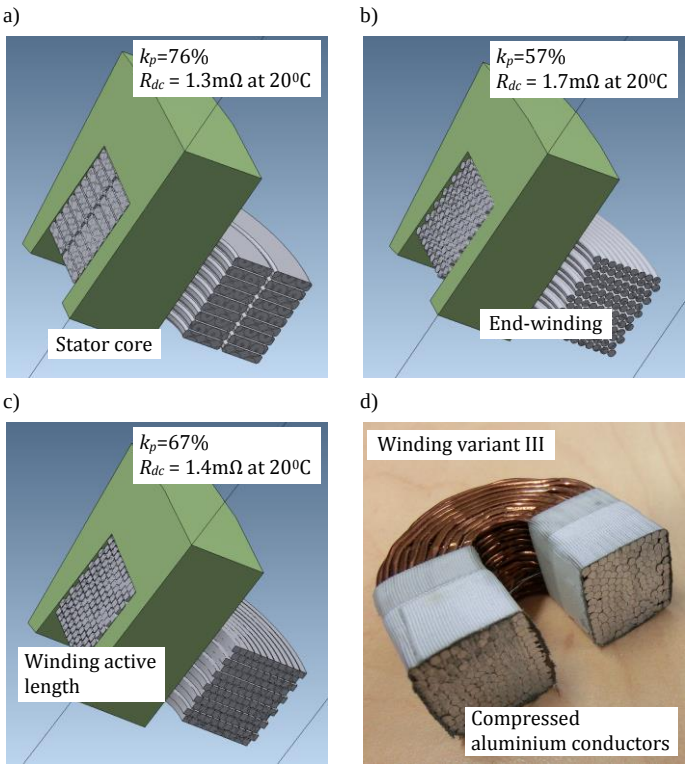

Fig. 2. Outline of the winding's coil constructions a) 1.9mm×8.3mm edge wound – winding variant I, b) 6×∅1.6mm multi-stranded wound –winding variant II, c) 7×∅1.6mm compressed multi-stranded wound –winding variant III, d) cross-section of a prototype coil with compressed conductors

coil construction with profiled rectangular conductors, winding variant I and a multi-stranded round conductor construction in uncompressed and compressed forms, winding variants II and III respectively, Figs. 2a, 2b and 2c. Fig. 2d presents a prototype of the multi-stranded and compressed coil cross-section cut-away reviling high conductor compaction, with the individual conductor's cross-section being deformed from the original round shape to a polygonal shape. Here, an individual preformed/compressed coil is formed in isolation on a custom build mandrel. After an initial winding stage, the coil is compressed using a coil former, which fully encompasses the coil body during the compression phase. The preformed/ compressed coil is then removed from the mandrel and is ready to be slotted into the stator core pack. It is important to note that the concept of a compressed coil construction has been researched by other authors [6], [12], [25]. Here, however the use of multi-stranded bundle of round conductors as opposed to a single round conductor per coil turn has been investigated in more detail.

The winding variant I provides the highest effective conductor fill factor among the winding variants considered in the analysis, k_p = 76%. Winding variants II and III have lower effective conductor fill factor and consequently higher dc resistance as compared with the winding variant I. It is important to note that dc resistance and/or conductor fill factor is not indicative of the winding power loss at ac operation when a wide range of rotational speeds/frequencies is considered [14]. The overall winding loss at ac operation is a fine balance between the dc and ac loss components for a required torque-speed envelope or duty-cycle.

In the analysis the effective conductor fill factor is defined as a ratio of the total conductor cross-section area to the overall coil cross-section area, which differs from the more commonly used definition, where the stator slot cross-section is used as a reference. Such a definition has been adopted here due to specifics of the winding construction, where the stator slot window is only partially occupied by the winding conductors.

The winding construction with a multi-stranded bundle, where a number of smaller gauge parallel conductors are used to form individual turns of the coil (winding variants II and III), has been considered here as it allows for the rotational ac power loss component to be reduced as compared with the edge-wound winding design counterpart (winding variant I). To further reduce the rotational ac power loss component, the winding body is placed lower in the stator slots and occupies approximately 80% of the complete slot depth/window. The rotational winding ac effect has been shown to be significant for machine designs with open-slot stator topology [14], which is the stator design adopted in the design-analysis of the starter-generator to enable low-cost winding manufacture and assembly. The main drawback of the multi-stranded winding assembly is the random placement of the individual strands, which might result in uneven power loss generation for individual coils within the winding [15]. The winding power loss issues related with the selected winding construction and manufacture techniques are discussed in detail in the following sections of the paper.

IV. Analysis

A series of design-analyses have been performed in order to establish the feasibility of the proposed machine topology at an early stage and to provide performance metrics. The analyses include electromagnetic finite element analysis (FEA) accounting for the power loss components at ac operation and thermal lumped-parameter equivalent-circuit analysis to assess the thermal behaviour of the design for the required operating cycle. The initial FEAs confirmed that the open-slot stator-winding arrangement is susceptible to elevated ac winding loss as a result of the rotating field generated by the PM rotor. To mitigate this effect the winding height is reduced, Figs. 1 and 2, which impacts the available conductor cross-section area within the stator slot thereby increasing dc resistance, however, the increase is minimised by the use of a compressed coil construction with a high effective fill factor when compared with more conventional winding methods.

A. Electromagnetic Model

To assure winding design with minimum power loss for the required torque-speed envelope or duty-cycle, a number of two- and three-dimensional (2D and 3D) FEAs of the winding variants discussed earlier have been carried out. The ac winding loss predictions have been performed using time stepping FEA where the winding coils are driven with 3-phase sinusoidal and balanced current waveforms in the case of the complete starter-generator assembly, Fig. 1, and 1-phase sinusoidal current waveform for the motorette models, Fig. 2. The individual winding conductors are represented within the FE model as

solid conductors linked with an external circuit defining the electrical connections between the winding conductors, coils and phases where appropriate. To emulate the random conductor lay for the winding variants II and III an irregular shape of bundles forming the individual winding's turns has been assumed as shown in Fig. 3. It is important to note that no transposition of the individual stands has been considered, i.e. all conductors are geometrically parallel in the plane of the winding.

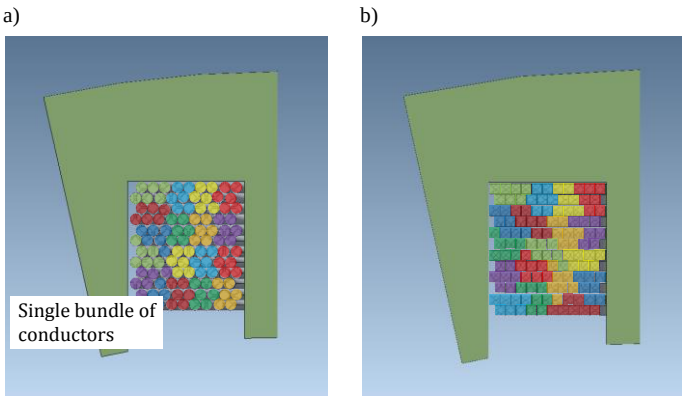

Fig. 3. Conductor's lay assumed in the FEAs a) winding variant II, b) winding variant III

The 'pancake' like geometry of the analysed starter-generator resulted in the end-winding dc resistance to be comparable with that of the active length region of the winding. To provide accurate winding loss prediction at ac operation for both the active length and end-winding regions a combination of 2D and 3D FEAs has been employed. 2D FE is used to analyse the complete starter-generator accounting for the active length winding loss contribution, whereas 3D FE is used to analyse the motorette assembly allowing for the end-winding loss to be derived. Also, the 3D FE is used to theoretically derive winding inductance accounting for the ac effects. The total winding loss at ac operation is a sum of the active length and end-winding losses:

$$P_{ac} = P_{ac\,al} + P_{ac\,ew} \quad , \qquad (1)$$

where $P_{ac\,al}$ and $P_{ac\,ew}$ refers to the active length and end-winding region respectively.

This decoupled approach allows for the winding loss to be derived in a computationally efficient manner as compared with direct 3D FEA, which is frequently found to be computationally prohibitive. It is important to note that the employed approach assumes that the ac rotational effect associated with the end-winding region is negligible.

In the FEA, the generated winding loss is determined from the Joule loss [14]. To account for the change in conductor resistivity with temperature, the following correction has been used:

$$\rho|_T = \rho|_{T_0}\big(1 + \alpha(T - T_0)\big), \quad , \qquad (2)$$

where $\rho|_{T_0}$ is the resistivity of aluminium conductors at T_0 = 20°C, $2.83\times10^{-8}\Omega$m and α is the temperature coefficient of resistance for aluminium is $4.30 \times 10^{-3}K^{-1}$. The FEA assumes constant conductor temperature T across the winding body.

The winding power loss data derived from the reduced number of FEAs has been used to inform a winding loss function for both the active length and end-winding regions. The winding loss function allows for accurate and computationally efficient loss update with excitation frequency, current amplitude and winding temperature, which is essential when considering derivation of the thermal operating envelope and/or the efficiency map for a particular torque-speed envelope or operating duty-cycle. The functional representation of the winding power loss proposed in [14] has been employed in this research:

$$\begin{aligned} P_{ac}|_T &= P_{dc}|_{T_0}\big(1 + \alpha(T - T_0)\big) \\ &+ P_{dc}|_{T_0}\frac{\left(\frac{R_{ac}}{R_{dc}}\right)_E\Big|_{T_0} - 1}{\big(1 + \alpha(T - T_0)\big)^{\beta}} \\ &+ P_{acR}|_{T_0}\frac{1}{\big(1 + \alpha(T - T_0)\big)^{\gamma}} \end{aligned} \quad , \qquad (3)$$

where

$$P_{dc}|_{T_0} = I^2 R_{dc}|_{T_0} \quad , \qquad (4)$$

$$\left(\frac{R_{ac}}{R_{dc}}\right)_E\Big|_{T,I} = \left(\frac{P_{ac} - P_{acR}}{P_{dc}}\right)\Big|_{T,I} \quad , \qquad (5)$$

and R_{dc} is the dc resistance of the winding β and γ are parameters that can be found by curve fitting (3) of the ac winding loss data for temperature T. It has been assumed here that T is the highest operating temperature considered for a device. P_{acR} is the winding loss at open-circuit operation from rotational effect. $(R_{ac}/R_{dc})_E$ defines the average winding power loss from excitation at ac operation and can be derived from hardware tests or FEAs assuming equivalent ac and dc excitation current, I, and fixed winding temperature, T, $(R_{ac}/R_{dc})_E|_{T,\,I} = (P_{ac}/P_{dc})_E|_{T,\,I}$ [16].

TABLE II. FEAs' DERIVED COEFFICIENT FOR THE POWER LOSS FUNCTION

Winding variant	Active length region		End-winding region	
	β_{al}	γ_{al}	β_{ew}	γ_{ew}
I	0.90	0.50	0.60	-
II	0.75	1.00	0.80	-
III	0.75	1.00	0.80	-

Table II includes coefficients β and γ derived from FEAs accounting for both the active and end-winding regions. It is important to remember that the rotational effect associated with the end-winding has been assumed to be negligible in this analysis, thus γ_{ew} is not derived.

The iron power loss has been estimated using specific loss data for NO20 (0.20mm thickness SiFe) provided by the steel manufacturer and FEAs with the modified Steinmetz approach. To accelerate the process of deriving the starter-generator's performance for multiple operating points, required to generate a complete torque-speed and efficiency map a technique proposed in [17] has been employed. The method is based on a coarse iron loss mapping with in-between set-point interpolation. The mechanical loss associated with frictional effects in the bearings and aerodynamic drag or windage within the machine body are not considered in the overall power loss balance. In particular, the bearing loss has been neglected as rotational movement for the starter-generator's rotor is provided by the existing transmition system of an internal combustion engine that the starter-generator is intended to be integrated with.

B. Thermal Model

A complete thermal model of the starter-generator has been built using the thermal lumped-parameters equivalent-circuit [18] method. The model accounts for the conduction, convection and radiation heat transfer mechanisms including the air-flow transition effects. Fig. 4 presents the thermal network used with horizontal and vertical circuit-branches representing axial and radial heat paths within the machine assembly respectively. It is important to note that the adopted model assumes periodic

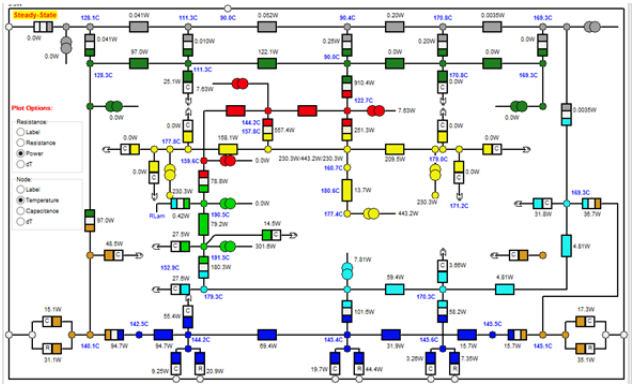

Fig. 4. Thermal lumped-parameter equivalent circuit model representation of the starter-generator assembly

a) b)

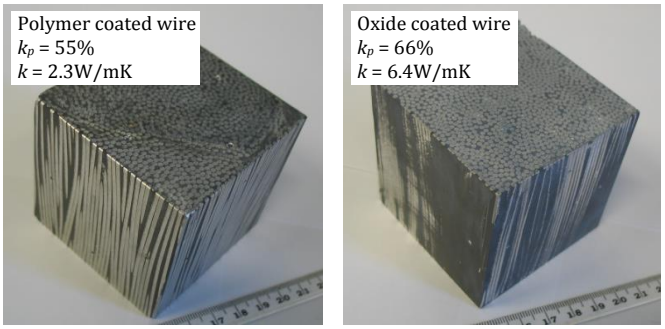

Fig. 5. Impregnated winding material samples representative of the multi-stranded coil construction used to measure thermal properties for the winding amalgam

symmetry over machine's circumference, i.e. each periodic stator-winding sector is identical in terms of power loss generated and heat transfer. The model's input power loss data has been accounted for by the use of techniques discussed in the previous section. To provide a degree of calibration for the thermal model, a number of tests have been carried out on winding amalgam material samples and a motorette assembly. The aim of the tests was to derive the thermal material properties for the representative winding amalgam samples and determine the quality of the conductive heat transfer path from the winding through the stator core pack into the heat sunk housing assembly. Details regarding the experimental setups used in the analysis are provided in the next section.

An initial sensitivity analysis has been performed using the thermal model to identify the main heat transfer paths and mechanisms together with construction/assembly nuances, which have a significant impact on the starter-generator thermal behaviour. The analysis confirmed that the main heat transfer path is provided by conduction from the impregnated stator-winding assembly to the heat sink housing. As this is the intended mechanism for evacuating heat from the starter-generator body, correct calibration of any interface thermal resistances from the stator-winding to the motor shaft were found to be crucial to the accuracy of the thermal model. The calibrated model is the basis for the analysis of the starter-generator's torque-speed envelope and efficiency maps for the analysed winding variants.

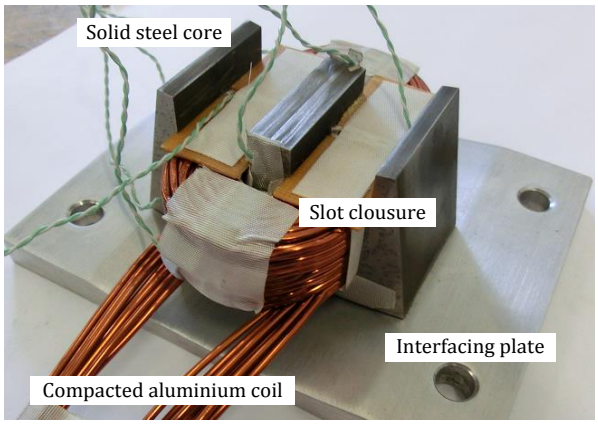

Fig. 6. Instrumented sector of the stator-winding assembly (motorette) prior to impregnation

C. Subassembly Hardware Tests

1) Winding Thermal Material Data Derivation

In order to improve the accuracy of the thermal predictions a number of winding material samples have been manufactured and the thermal properties measured experimentally to give the thermal conductivity and specific heat capacity of the composite winding region. Fig. 5 presents some of the winding material samples considered, with alternative wire coatings and varying conductor fill factor. The material testing procedure used in this analysis is analogous to that presented in [19], [27]. A heat flux meter has been used to derive a set of thermal conductivities accounting for the winding amalgam anisotropy. The specific

TABLE III. EXPERIMENT INFORMED THERMAL CONDUCTIVITY DATA FOR IMPREGNATED WINDING VARIANTS

Winding variant	k_x [W/m K]	k_y [W/m K]
I	2.36	1.99
II	0.76	0.76
III	2.32	2.32

heat capacity has been found from calorimetric tests on alternative winding samples. Table III lists thermal conductivity data informed from tests on appropriate impregnated winding material samples for the analysed winding variants. When reviewing the data, it is evident that 'good' conductor compaction results in improved winding thermal conductivity. This is particularly prominent when comparing winding variants with the same conductor profile without and with conductor compression, winding variant II and III respectively. It is worth noting that winding variant with profiled rectangular conductors (winding variant I) exhibits a degree of thermal anisotropy, which results from the conductor profile/arrangement. Here, thermal conductivity in *x* and *y* axes are associated with heat transfer into the tooth and stator back iron correspondingly.

2) Heat TransferAnalysis

To provide an insight into the heat transfer from the starter-generator's stator-winding assembly to the heat sunk housing, a dc test was carried out on the motorette setup. The motorette body was mounted on a liquid-cooled aluminum interfacing plate with an appropriate retention system to emulate the housing assembly. Fig. 2 presents the motorette body together with the interfacing plate prior to impregnation and final assembly. The motorette setup is then placed in a thermally insulated chamber and instrumented with type-K thermocouples. Excitation for the motorette winding is provided by a dc power supply, and the fixed temperature of the cold plate is controlled by a cooling unit. The temperature within the motorette assembly was monitored at a number of points including the winding, laminated core pack, aluminum interfacing plate and cold plate. The measurements were taken for several excitation currents, and the averaged test data was used to calibrate the thermal model.

TABLE IV. EXPERIMENT INFORMED EQUIVALENT WINDING TO STATOR THERMAL CONDUCTANCE

Winding variant	h_c [W/m^2 K]
I	70.8
II	103.8
III	129.8

The data from dc thermal tests allows for an equivalent winding to stator thermal conductance to be derived [23], [26], [29]. This provides initial information regarding the effectiveness of heat evacuation from the winding body for the analysed winding arrangements, Table IV. Here, the winding variant III provides the highest thermal conductance and consequently the best dissipative heat transfer from the winding body. This results from 'good' winding thermal conductivity and improved winding to stator core pack contact thermal resistance.

3) Power Loss Measurements

In order to evaluate the impact of the manufacturing repeatability of the individual winding's coils on the ac winding loss, an experimental approach based on impedance analysis has been employed. Fig. 7 presents the testing setup, which includes a precision impedance analyser, laminated stator core pack and a coil under test. The impedance analysis allows the ac winding effects associated with the excitation, $(R_{ac}/R_{dc})_E$, to be quantified. In particular, a deviation between the coil

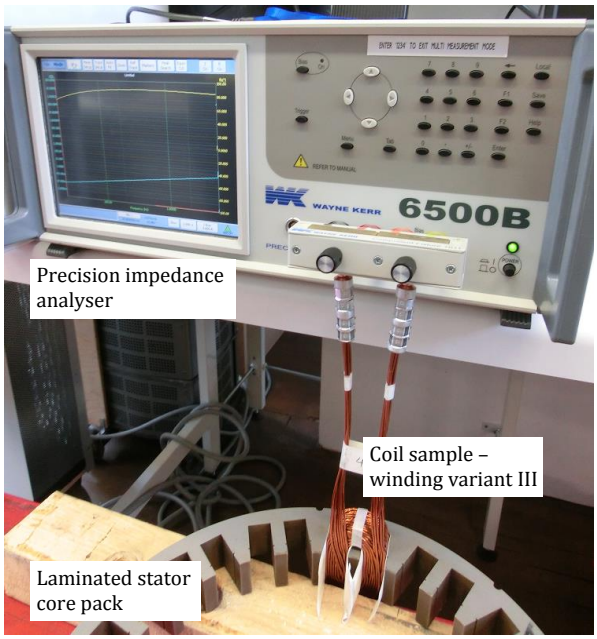

Fig. 7. Experimental setup used to evaluate ac excitation loss and winding inductance

samples is expected due to the random placement of the individual coil strands and bundles for the winding constructions with multi-stranded conductors (winding variants II and III) . In addition, the testing approach allows for the measurements to be performed in a repeatable and timely manner, which is desirable when measurements for a large number of coils is considered. Further to the experimental evaluation of the ac winding effects, the per coil inductance has been derived from the impedance measurements.

V. RESULTS

The prototyping efforts have been focused mainly on the winding construction with compacted conductors (winding variant III) as the least explored concept among the winding variants considered in this research. The experimental results included in this section are limited to winding variant III only, whereas theoretical work accounts for all the alternative winding arrangements considered in the research to provide a broader insight into the design choices.

As the analysed starter-generator has a relatively short active length, the end winding contribution to the overall winding has been found prerequisite of making informed design decisions. Initial analyses have focused on identifying the end winding inductance, which was essential for deriving the theoretical power output capability of the starter-generator at the higher end of the operating speeds. The theoretical predictions suggest that the end-winding inductance is 0.45 of the overall winding inductance. The FE predicted phase winding inductance is 13.5μH as compared with the measured 14.7μH showing good correlation. It is important to note that the inductance analysis refers to the stator-winding assembly only, and the overall winding inductance for the complete machine assembly is likely to be higher due to the presence of the rotor structure. The mutual coupling between adjacent coils/phases is negligible here due to the modular winding topology, which provides magnetic separation for the winding modules/coils. In general however, the coupling effect needs to be accounted for [28]. In addition, the 3D FEA used to derive the inductance does not account for any frequency dependant ac effect in the laminated stator core pack. It has been reported in the literature that the end winding inductance contribution is affected by the stator core end-winding effects at ac operation [20]. These result in a reduction of end-winding inductance at higher excitation frequencies. Furthermore, it has been shown that the winding inductance reduces with increase of the excitation frequency due to winding ac effects [21]. To provide an insight into these effects a number of measurements have been taken using the approach described in the previous section. Fig. 8 presents the measured inductance for the individual winding coils illustrating a degree of discrepancy between the coils as well as a reduction of inductance with the excitation frequency. The inductance reduction is negligibly small and equal to approximately 1% at 1kHz for both experimentally and theoretically derived data. Note that 1kHz refers to the fundamental excitation frequency and represents the top end of the starter-generator's operating envelope. The averaged coil inductance has been derived from a

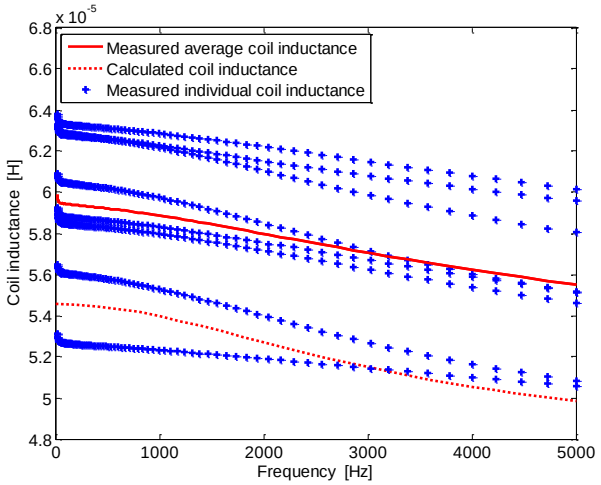

Fig. 8. Measured inductance for the individual winding's coils vs. excitation frequency for winding temperature T= 20^{0}C

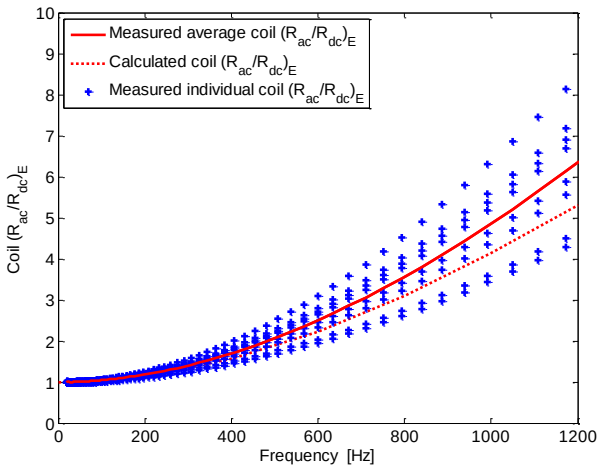

Fig. 9. Measured and calculated $(R_{ac}/R_{dc})_E$ for the individual winding's coils vs. excitation frequency for winding temperature T= 20^{0}C

a)

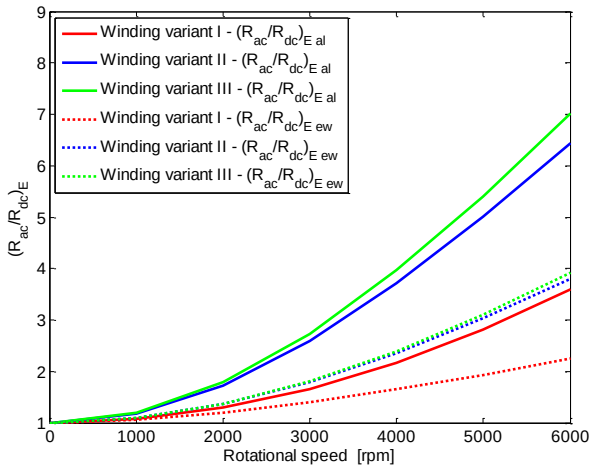

Fig. 10. Calculated $(R_{ac}/R_{dc})_E$ for the active length and end winding regions vs. rotational speed at winding temperature T= 20^{0}C and I_{ph} = 400A$_{rms}$

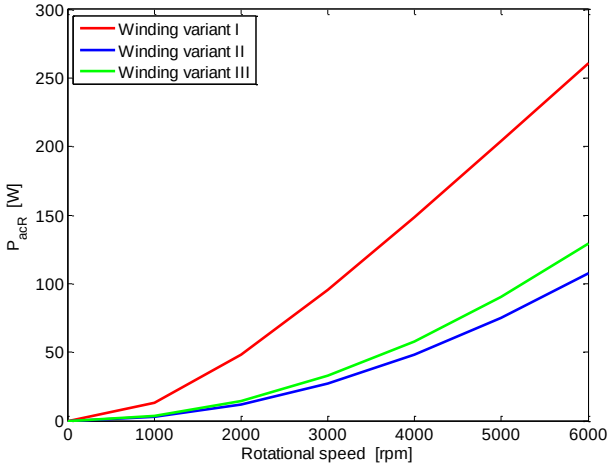

Fig. 11. Calculated winding open-circuit power loss P_{acR} vs. rotational speed at winding temperature T= 20^{0}C

number of measurements taken on a test batch of coils. Clearly, the inductance discrepancies between the individual winding coils are undesirable, in particular when parallel paths/connections between the individual coils per phase are considered. Regardless of the coil manufacture issues, a detailed analysis of the complete starter-generator has shown that the winding inductance does not limit the power output rating at the higher end of the operating speeds.

Similar as in the case of the inductance analysis, a degree of discrepancy between the individual winding coils is expected for the ac winding power loss. To quantify that concern, the $(R_{ac}/R_{dc})_E$ ratio has been derived for the same test batch of coils. Fig. 9 presents $(R_{ac}/R_{dc})_E$ versus excitation frequency at a fixed temperature, $T = 20^0$C. The measured results suggest significant differences between the coils with $(R_{ac}/R_{dc})_E$ in a range from 3.6 to 6.8 at 1kHz, which is approximately 86% variation for these extremities. This clearly has important implications regarding the starter-generator performance with uneven power loss generation across the winding coils. It is evident that an improved and more repeatable manufacture process for the winding is required to make the multi-stranded compacted winding construction a valiable solution.

It is important to note that the initial test batch of coils has been manufactured to meet a limited number of design requirements, which included a fixed number of turns and outer dimensions with the lowest possible dc resistance practically achievable. No precision conductor lay was considered for the batch of test coils. A comparison between averaged $(R_{ac}/R_{dc})_E$ form measurements and FEAs has also been included in Fig. 8 suggesting that theoretical predictions of the winding loss provide good starting point for more detailed design considerations.

Fig. 10 presents FE predicted $(R_{ac}/R_{dc})_E$ for the winding variants considered in the analysis with distinction between the winding active length $(R_{ac}/R_{dc})_{E\ al}$ and end $(R_{ac}/R_{dc})_{E\ ew}$ regions. The results suggest that the winding variant I assures the lowest ac excitation related effects among the analysed winding constructions. For winding variants II and III the ac excitation effects are similar. However, as winding version III provides lower dc resistance than winding version II, the overall winding power loss is lower for the winding construction with compressed multi-stranded bundles (winding variant III). Also, the results suggest that the ac end-winding effects are non-negligible and need to be accounted for in the design considerations to provide accurate power loss predictions. Fig. 11 shows the contribution of the rotational ac effect given by winding power loss at open-circuit operation, P_{acR}. In this case the results suggest that winding variant I has the highest winding loss from rotational ac effects, whereas winding variant II assures the lowest winding loss at open-circuit operation. It is important to note that the overall winding loss depends on the operating envelope and duty cycle with both excitation and rotational effects contributing differently for the lower-speed high-torque and high-speed low-torque regions. Clearly, in order to down select the most promising, low-loss winding candidate, an analysis of the complete operating envelope including intended operating duty is required. Fig. 12 presents target torque-speed envelope for both the continuous and peak transient operating modes. The consecutive efficiency maps

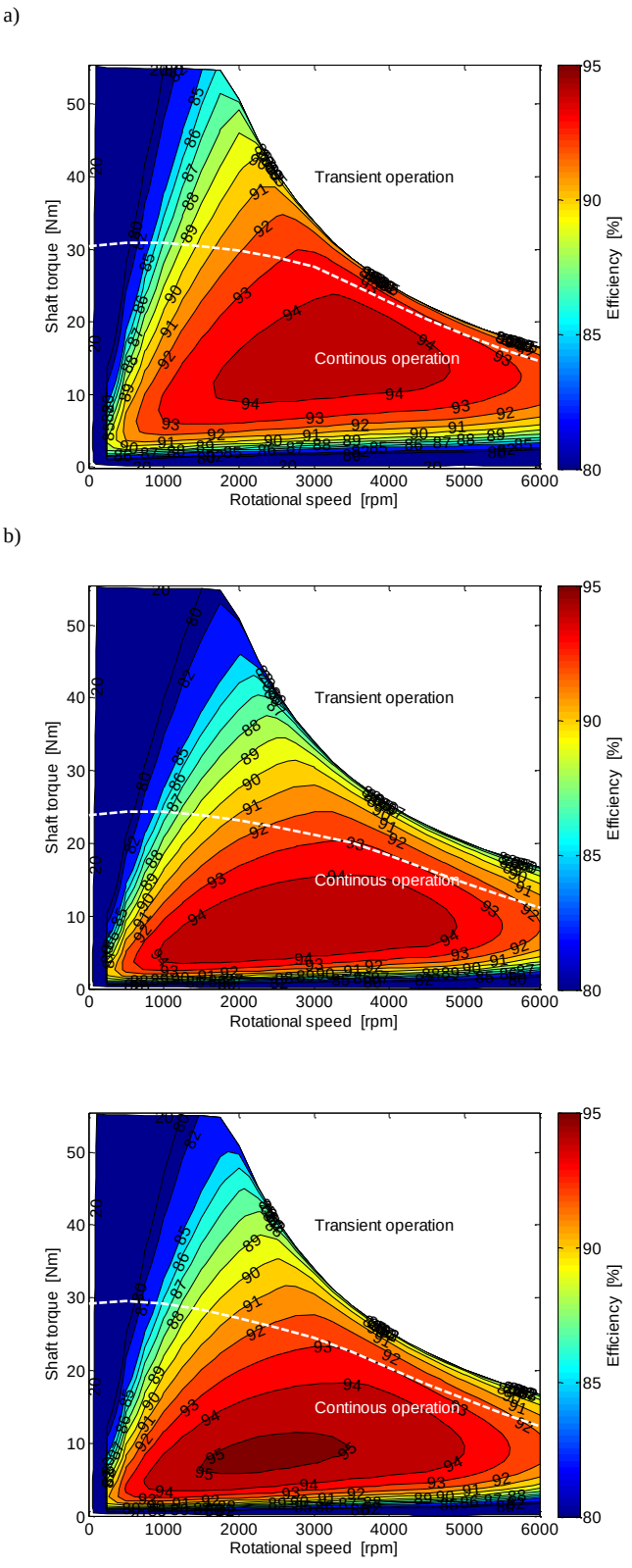

Fig. 12. Target torque-speed envelope together with efficiency map; a) winding variant I, b) winding variant II, c) winding variant III

shown in Fig. 12 refer to the alternative winding constructions considered in the research. For the efficiency analysis, it has

been assumed that all the machine active components are at fixed temperature of 120^0C. When analysing the efficiency maps it is evident that winding version I offers relatively narrow window of 'high' efficiency operation, 94%, set between 1500rpm and 4500rpm as compared with winding version II and III, where the 'high' efficiency operating region is broader and set between 750rpm and 5000rpm. However, winding variant I offers 'high' efficiency at 'high' torque operation. Also, the theoretical predictions suggests that winding version III provides the highest efficiency, 95%, among the analysed variants. The continuous operating envelope is also indicated in Fig. 11 with a dashed line. Here, the winding temperature limit has been set to 160^0C with machine housing at 65^0C and 6.5l/min coolant flow for the water jacket. It is clear that the winding variant I assures the widest continuous operating envelope meeting the design targets, whereas winding version II underperforms here, with the generated torque 20% lower than the design target. Winding version III provides torque which is marginally lower than the design requirement.

The presented efficiency and operating envelope analyses provide more detailed insight into the machine performance with the alternative winding constructions. However, as in the analysed case the intended duty cycle is a combination of continuous and peak transient operation, an analysis of the machine performance for a representative operating cycle would enable more definitive information regarding the design choices to be established. Fig. 13 presents a representative operating cycle assumed in the analysis revealing the transient nature of operation intended for the machine design. Table V lists the averaged machine performance measured, averaged over the operating cycle shown in Fig. 13. The calculated results include efficiency and power loss data suggesting that winding variant I provides the best performance for the intended operating duty cycle. In contrast, winding version II has the poorest performance measures as compared with counterparts I and III. Clearly the intended operating duty has a significant impact on the design decisions and has to be included in the design considerations, particularly if transient overload operation is envisaged.

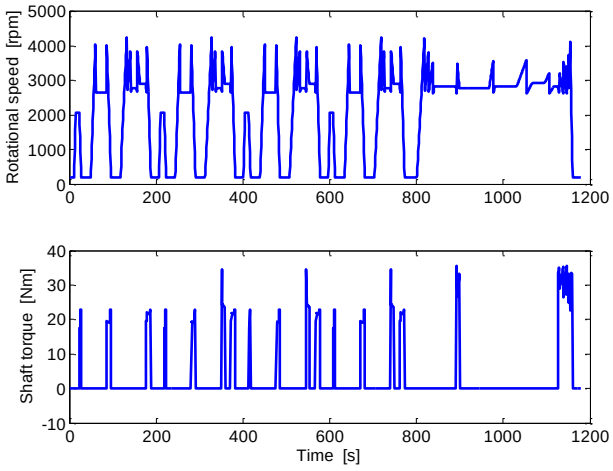

Fig. 13. A representative operating cycle assumed in the analysis; time variation of the rotational speed and shaft torque

TABLE V. MACHINE AVERAGED PERFPRMANCE MEASURES OVER THE REPRESENATIVE OPERATING CYCLE, SEE FIG. 12

Performance measure	Winding version		
	I	II	II
Averaged efficiency [%]	91.3	88.9	90.1
Total power loss [Wh]	39.4	45.2	42.1
Winding power loss [Wh]	27.8	33.6	30.5
Core power loss [Wh]	11.6	11.6	11.6

In this research the final design choice regarding the winding construction will be made based on the predicted performance measures and 'design goodness' satisfying the 'design for manufacture' and 'design for cost' design paradigms, which will be investigated in the authors further research.

VI. CONCLUSIONS

This paper presents results from a study on an integrated brushless PM starter-generator. The original design remit was to incorporate cost effective materials and simple manufacturing and assembly methods. The selected topology is a radial-flux machine with an open-slot modular aluminium winding and an inner rotor with surface mounted ferrite PMs. A Halbach array is used in the rotor construction to realise a relatively high magnet loading, 0.4T, from the ferrite magnets. The open-slot single layer modular topology allows for the coils to be pre-formed and a high volume of conductor can be incorporated to offset the poorer resistance of aluminium. As a result the achieved electrical loading is comparable to that of a more conventional distributed winding using copper conductors.

The employed analyses process used in the design combine theoretical and experimental approaches. 2D and 3D electromagnetic FEA has been employed to define the dimensions of the stator iron and the magnet array. This FEA was also used to set the winding turns and to establish the machine torque constant, emf and inductance. 3D FEA was necessary to appraise the contribution of the end winding; the contribution of the end winding to the overall inductance and loss is significant due to the short active length. Further, the electromagnetic analyses were used to investigate in more detail the distribution of loss in the stator with an emphasis on ac winding loss effects. Functional relationships are used to capture the variation of loss with temperature and operating frequency. This methodology has the benefit of reducing the number of FEA required to characterise the design over a full operating envelope to those required to identify the coefficients in the loss expressions. A lumped-parameter thermal equivalent-circuit model was formulated to assess the thermal behaviour of the design over the required operating cycle, using the FEA derived loss data as input. The resultant coupled electromagnetic and thermal analysis have been applied to determine the continuous output capability within the winding, the thermal constraints and to yield an efficiency map. The initial experimental work used thermal tests on sub-assembly 'motorettes' to calibrate the thermal model. The bulk thermal properties of the winding regions were obtained using heat flux and calorimetric measurements. The thermal resistances across the critical interfaces between the winding and core pack and from the core

pack to casing were also estimated from experiment. Electrical tests on the preformed coils were also undertaken. The initial results have shown close correlation between FEA calculated inductances and ac loss factor and measured data. The use of sub-assemblies to calibrate and validate the modelling work is proven to be a valuable and cost effective approach.

The performances of three alternative winding constructions have been compared, one formed from edge wound rectangular conductors, one from multiple strands of parallel conductors and a third compressed version of the multi-stranded arrangement. A high effective conductor fill factors was achieved in the compressed multi-stranded coils, being only 10% less than that of an ideal rectangular conductor arrangement. The analyses indicated that the rectangular and compressed multi-stranded coil constructions would deliver the required performance of the application, whereas an un-compressed multi-stranded coil construction would not. The ac loss resulting from rectangular and the multi-stranded coils are shown to be very different, the 'edge wound' rectangular conductors have the lowest excitation related ac loss, whereas the multi-stranded arrangement has much lower rotor induced loss.

Experimental measurements on the compressed multi-stranded coil construction indicated that the ac losses, and to a lesser extent the inductance, is highly sensitive to the conductor lay. Tests across a batch of eight coils indicated an ac loss factor spread between 3.6 to 6.8 at 1kHz and an approximately 20% variation in inductance. The random nature of the 'in-hand' method of winding parallel conductor turns means that the conductor lay cannot be precisely defined and a controlled conductor placement method of manufacture is required in the future.

ACKNOWLEDGMENT

The research presented in this paper has been funded by the UK government under the Innovate UK Evoque-E project. The University of Bristol wish to thank Infolytica Europe and Motor Design Limited for providing the software used in this research.

REFERENCES

[1] S. J. Galioto, P. B. Reddy, A. M. El-Refaie, "Effect of Magnet Types on Performance of High Speed Spoke Interior Permanent Magnet Machines Designed for Traction Applications," *IEEE Energy Conversion Congress and Exposition*, (*ECCE2014)*, Pittsburgh, Pennsylvania, USA, 14-18 September 2014, pp. 4513-4522.

[2] Y. Takano, M. Takeno, T. Imakawa, A. Chiba, N. Hoshi, M. Takemoto, S. Ogasawara, "Torque Density and Efficiency Improvements of a Switched Reluctance Motor Without Rare-Earth Material for Hybrid Vehicles," *IEEE Energy Conversion Congress and Exposition, (ECCE2010)*, pp. 2653-2659, September 2010.

[3] M. Takeno, A. Chiba, N. Hoshi, S. Ogasawara, M. Takemoto, M. A. Rahman, "Test Results and Torque Improvement of the 50-kW Switched Reluctance Motor Designed for Hybrid Electric Vehicles," *IEEE Transactions on Industry Applications*, vol. 48, no. 4, pp. 1327-1334, July/August 2012.

[4] M. Ferrari, N. Bianchi, A. Doria, E. Fornasiero, "Design of Synchronous Reluctance Motor for Hybrid Electric Vehicles," *IEEE International Electrical Machines and Drives Conference*, *(IEMDC2013)*, pp. 1058-1065, May 2013.

[5] M-F Hsieh, Y-C Hsu, D. G. Dorell, "Design of a Large-Power Surface-Mounted Permanent-Magnet Motors Using Postassembly Magnetization, " *IEEE Transactions on Industrial Electronics*, vol. 57, no. 10, pp. 3376-3384, October 2010.

[6] A. G. Jack, B. C. Mecrow, P. G. Dickinson, D. Stephenson, J. S. Burdess, N. Fawcett, J. T. Evans, "Permanent-Magnet Machines with Powdered Iron Cores and Prepressed Windings," *IEEE Transactions on Industry Applications*, vol. 36, no. 4, pp. 1077-1084, July/August 2000.

[7] B-T Kim, "Design of New Type Universal Motor Using Soft Magnetic Composites," *Journal of Electrical Engineering and Technology*, vol. 1, no. 2, pp. 211-115, 2006.

[8] R. Wrobel, P. H. Mellor, "Design Considerations of a Direct Drive Brushless Machine with Concentrated Windings," *IEEE Transactions on Energy Conversion*, vol. 23, no. 1, pp. 1 – 8, March 2008.

[9] R. Wrobel, P. H. Mellor, D. Holliday, "Thermal Modelling of a Segmented Stator Winding Design," *IEEE Transactions on Industry Applications*, vol. 47, no. 5, pp. 2023 – 2030, September – October 2011.

[10] R. Wrobel, P. H. Mellor, N. McNeill, D.A. Staton, "Thermal Performance of an Open-Slot Modular-Wound Machine with External Rotor," *IEEE Transactions on Energy Conversion*, vol. 25, no. 2, pp. 403 – 411, June 2010.

[11] R. Wrobel, D. Salt, N. Simpson, P. H. Mellor, "Comparative Study of Copper and Aluminium Conductors – Future Cost Effective PM Machines," 7th IET International Conference on Power Electronics, Machines and Drives, *(PEMD 2014)*, Manchester, UK, pp. 1 -6, April 2014.

[12] J. D. Widmer, C. M. Spargo, G. J. Atkinson, B. C. Mecrow, "Solar Plane Propulsion Motors With Precompressed Aluminum Stator Windings", *IEEE Transactions on Energy Conversion*, vol. 29, no. 3, pp. 681 – 688, September 2014.

[13] J. Goss, R. Wrobel, P. H. Mellor, D. Staton, "The design of AC permanent magnet motors for electric vehicles: A design methodology", Electric Machines & Drives Conference (*IEMDC 2013*), 2013, pp. 871-878.

[14] R. Wrobel, D. Staton, R. Lock, J. Booker, D. Drury, "Winding Design for Minimum Power Loss and Low-Cost Manufacture in Application to Fixed-Speed PM Generator", *IEEE Transactions on Industry Applications*, vol. 51, no. 5, pp. 3773 – 3782, September-October 2015.

[15] P. Mellor, R. Wrobel, D. Salt, A. Griffo, "Experimental and Analystical Determination of Proximity Losses in a High-Speed PM Machine", *IEEE Energy Conversion Congress and Exposition, (ECCE2013)*, pp. 3504-3511, September 2013.

[16] R. Wrobel, D. E. Salt, A. Griffo, N. Simpson, , P. H. Mellor, "Derivation and Scaling of Copper Loss in Thermal Modeling of Electrical Machines ," *IEEE Transactions on Industrial Electronics*, vol. 61, no. 8, pp. 4412 – 4420, August 2014.

[17] J. Goss, M. Popescu, D. Staton, R. Wrobel, J. Yon, P. Mellor, "A Comparision Between Maximum Torque/Ampere and Maximum Efficiency Control Strategies in IPM Synchronous Machines," *IEEE Energy Conversion Congress and Exposition, (ECCE2014)*, pp. 2403 - 2410, September 2014.

[18] Motor-CAD V6 Maual, Motor Design Ltd, 2011.

[19] N. Simpson, R. Wrobel, P. H. Mellor, "Estimation of Equivalenet Thermal Parameters of Impregnated Electrical Windings," *IEEE Transactions on Industry Applications*, vol. 49, no. 6, pp. 2505 – 2515, November/December 2013.

[20] R. Lin, A. Arkkio,"Calculation and Analysis of Stator End-Winding Leakage Inductance of an Induction Machine," IEEE Transaction on Magnetics, vol. 45, no. 4, pp. 2009 – 2014, April 2009.

[21] D. C. Hanselman, W. H. Peake, "Eddy-Currents Effects in Slot-Bound Conductors," *Electric Power Applications - IEEE Proceedings*, vol. 142, no. 2, pp. 131-136, 1995.

[22] R. P. Wojda, M. K. Kazimierczuk, "Analytical Winding Foil Thickness Optimisation of Inductors Conducting Harmonic Currents," I*ET Power Electronics*, vol. 6, no. 5, pp. 963-973, May 2013.

[23] R. Wrobel, S. J. Wiliamson, N. Simpson, S. Ayat, J. Yon, P. H. Mellor, "Impact of Slot Shape on Loss and Thermal Behaviour of Open-Slot Stator Windings", *IEEE Energy Conversion Congress and Exposition, (ECCE2015)*, pp. 4433 – 4440, September 2015.

[24] S. Ayat , R. Wrobel, J. Goss, D. Drury, "Experiment Informed Methodology for Thermal Design of PM Machines," *11th International Conference on Ecological Vehicles end Renewable Energies*, (*EVER 2016)*, pp. 1 – 7, April 2016, pp. 1-7.

[25] J. Widmer, R. Martin, B. Mecrow, "Pre-Compressed and Stranded Aluminium Motor Windings for Traction Motors," IEEE Transactions on Industry Applications, vol. 52, no. 3, pp. 2215 – 2223, May/June 2016.

[26] R. Wrobel, S. J. Williamson, J. D. Booker, P. H. Mellor, "Characterising the 'in situ' Thermal Behaviour of Selected Electrical Machine Insulation and Impregnation Materials," *IEEE Transactions on Industry Applications, (early access article).*

[27] S. Ayat , R. Wrobel, J. Goss, D. Drury, "Estimation of Equivalent Thermal Conductivity for Impregnated Electrical Windings Formed from Profiled Rectangular Conductors," *IET 8th International Conference on Power Electronics, Machines and Drives, (PEMD 2016),* pp. 1 – 6, April 2016.

[28] A. Taieb Brahimi, A. Foggia, G. Meunier, "End Winding Reactance Computation using a 3D Finite Element Program", *IEEE Transactions on Magnetics*, vol. 29, no. 2, March 1993, pp. 1411- 1414.

[29] N. Simpson , R. Wrobel, J. D. Booker, P. H. Mellor, "Multi-Physics Experimental Investigation into Stator-Housing Contact Interface," *IET 8th International Conference on Power Electronics, Machines and Drives, (PEMD 2016),* pp. 1 – 6, April 2016.